Journal of the Korean Magnetic Resonance Society **2019**, *23*, 12-19

DOI 10.6564/JKMRS.2019.23.1.012

Measuring T_1 contrast in ex-vivo prostate tissue at the Earth's magnetic field

Sangwon Oh[1,*], Jae Ho Han[2], Ji Eun Kwon[2], Jeong Hyun Shim[1], Seong-Joo Lee[1], Seong-Min Hwang[1], Ingo Hilschenz[1], and Kiwoong Kim[1]

[1]Ultra-low Magnetic Field Team, Korea Research Institute of Standards and Science, Daejeon, Republic of Korea, 34113
[2]Department of Pathology, Ajou University School of Medicine, Suwon, Republic of Korea, 16499

Received Mar 8, 2019; Accepted Mar 17, 2019

Abstract A former study has shown that the spin-lattice relaxation time (T_1) in cancerous prostate tissue had enhanced contrast at an ultra-low magnetic field, 132 μT. To study the field dependence and the origin of the contrast we measured T_1 in pairs of ex-vivo prostate tissues at the Earth's magnetic field. A portable and coil-based nuclear magnetic resonance (NMR) system was adopted for T_1 measurements at 40 μT. The T_1 contrast, $\delta = 1 - T_1$ (more cancer)/T_1(less cancer), was calculated from each pair. Additionally, we performed pathological examinations such as Gleason's score, cell proliferation index, and micro-vessel density (MVD), to quantify correlations between the pathological parameters and T_1 of the cancerous prostate tissues.

Keywords ultra-low field NMR, portable NMR, T_1 contrast, prostate cancer

Introduction

Prostate cancer is one of the most frequent causes of cancer-related death in the world. However, the 5-year survival rate of prostate cancer patients in a local or regional stage was almost 100% in 2017, suggestive of the importance of early detection of prostate cancer.[1] Digital rectal examination (DRE) results and serum prostate-specific antigen (PSA) levels are generally used for prescreening of prostate cancer, and transrectal ultrasound (TRUS) -guided sextant biopsy is a commonly accepted method to diagnose prostate cancer.[2] However, TRUS-guided biopsy has a low detection sensitivity (≈ 48%) and the invasive modality needs to be improved.[3]

Magnetic resonance imaging (MRI) of prostate, introduced in the 1980s, has improved the cancer detection.[4,5] Moreover, recent multi-parametric MRI - T_1 weighted imaging, T_2 weighted imaging, diffusion weighted imaging, dynamic contrast enhanced imaging, and magnetic resonance spectroscopic imaging - was reported to show 93% sensitivity in a study involving 576 participants.[3] Additionally, hyper-intensity or hypo-intensity in non-cancerous tissue due to biopsy-related hemorrhage, hormone therapy, prostatitis, and post-radiation fibrosis can be distinguished by multi-parametric MRI.[6]

The role of T_1 weighted imaging in prostate cancer imaging has been usually limited to locating biopsy-related artifacts such as hemorrhage. Busch et al. showed that increased T_1 contrast in cancerous prostate tissue could locate prostate tumors without contrast agents at 132 μT by utilizing superconducting quantum interference device (SQUID) -based MRI.[7] The increased T_1 contrast implied that T_1 weighted imaging in ultra-low magnetic fields could be an alternate technique to dynamic contrast enhanced imaging for patients with impaired renal function. To

*Address correspondence to: **Sangwon Oh,** Ultra-low Magnetic Field Team, Korea Research Institute of Standards a nd Science, Daejeon, Republic of Korea, 34113, Tel: 82-42-604-1117, E-mail: sangwon.oh@kriss.re.kr

obtain the best performance in ultra-low field T_1 weighted imaging, the T_1 contrast in various fields and T_1 decrease in cancerous prostate tissue need to be understood.

Here in this paper we performed T_1 measurements in prostate tissue at the Earth's magnetic field with a portable and coil-based NMR system and found an increased T_1 contrast in cancerous prostate tissue. Additionally, pathological examinations such as Gleason's score, cell proliferation index, and micro-vessel density (MVD) were performed to understand the correlations between T_1 and prostate cancer.

Experimental Methods

The coil-based NMR system, lower signal to noise ratio (SNR) but cryogenics free, was installed in a doctor's office, where the Earth's magnetic field was 40 μT. Terranova-MRI system (Magritek, Wellington, New Zealand) was modified to improve the low SNR. A new pre-polarizing coil (B_p) was wound to generate a pre-polarizing magnetic field of 50 mT at 6 A. The B_p coil was a multiple-layer (13 layers) solenoid, with a total number of turns of 1040. The inner radius, outer radius, and length were 32, 50, and 120 mm, respectively. The resistance and self-inductance of the B_p coil were 2.6 Ω and 37 mH. A new transmitter/receiver coil (B_1) coil was also wound to handle a smaller sample volume of 30 ml. The B_1 coil was a multiple-layer (22 layers) solenoid which total number of turns was 7260. The inner radius, outer radius, and length were 15, 23, and 100 mm, respectively. The resistance was 320 Ω and self-inductance was 628 mH. The quality factor of the B_1 coil at 1650 Hz was approximately 10. The B_P and B_1 coils were wrapped with nylon tube and cold de-ionized water (18 – 20 °C) was continuously circulated through the tube to cool them down. Thus, the temperature in the sample space was maintained at 25 ± 0.5 °C during the measurements. Additionally, the coils were placed in a Faraday cage, made of 8 mm thick aluminum with the dimensions of 500 × 500 × 500 mm^3. The cage was not grounded and the signal distortions due to the eddy current was negligible. The cage reduced ambient rf noise in the hospital by 10 dB compared to that without the cage.

A spin-echo based pulse sequence was used for T_1 measurements, Fig. 1. The B_P pulse was switched on to increase the magnetization along the axial direction of the B_P coil (z-axis) for 2 s and ramped down adiabatically.[8] During the ramp down the magnetization aligned along the Earth's magnetic field (x-axis) and spins relaxed back to the equilibrium state (T_1 relaxation) during t_{delay}. After t_{delay} a spin echo sequence was applied. To minimize rf phase mismatch we set the duration of the 90° pulse to multiples of the inverse of the Larmor frequency.[9] B_0 = 40 μT, B_P = 50 mT, t_{delay} = 30 – 200 ms (16 – 20 different delays), and 2τ (echo time) = 18 ms were selected. The sequence was repeated 96 time due to low SNR, approximately 10 after 96 averages, and it took 2 hours to finish a single T_1 measurement.

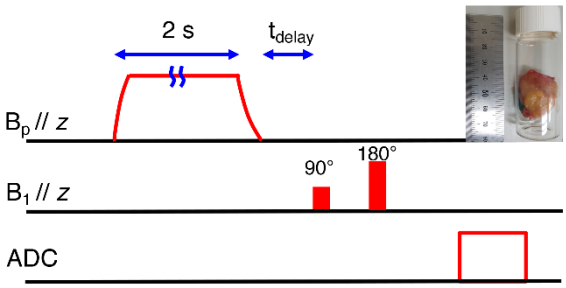

Figure 1. An NMR pulse sequence for T_1 measurements. A pre-polarizing magnetic field (B_p = 50 mT) was applied for 2 s to enhance the magnetization and then ramped down adiabatically, aligning the magnetization along the Earth's magnetic field (x-axis). A representative sample in a vial is shown in the inset.

In this study, fifteen pairs of prostate tissue specimens were investigated. Each pair consisted of a part of the right (RT) and left (LT) side of a whole prostate gland. After serial coronal sections of 8-mm thick prostatectomy specimen, one of the tissues was bisected into RT and LT for T1 measurement (Fig. 1). The dimension of the trimmed tissues was nominally ~ 30 × 10 × 8 mm^3, with a variation in thickness (width or length) of around ± 1 (5) mm. Specimen RT or LT were randomly chosen for sequential T_1 measurements and the tissue samples were kept in an air tight sample

holder during the measurement as an inset in Fig. 1. Additionally, we measured T_1 at two different times after the surgeries, within 30 minutes ("Fresh") and after 15 hours ("+15 Hrs"), to investigate the effect of sample degradation. Delayed ("+15 Hrs") samples were kept at 4 °C for 14.5 hours before the experiments and let them warm up to 25 °C for 30 minutes prior to the measurement. This research was approved by the Institutional Review Board of Ajou hospital.

Biological and geological samples are well-known for multiple nuclear relaxation times due to the heterogeneous nearby microstructures.[10,11] Due to the macroscopic sample size and inhomogeneities of the tissues, conventional single exponential fit was not adequate to identify the correct T_1 from the measurements. Instead, we adopted one-dimensional fast Laplace inversion (FLI) to determine the T_1 distribution in the sample and the distribution was then fitted to double Gaussian function to determine T_1 of cancerous prostate.[12,13] We briefly introduce the algorithm here and more details can be found in Ref. 12 and 13.

$$M(t_{de}) = \int \exp\left(-\frac{t_{de}}{T_1}\right) F(T_1) dT_1 + \varepsilon(T_1) \qquad (1)$$

The experimental data (M) at the time delay (t_{de}) can be expressed as in Eq. (1) where $F \geq 0$ for any T_1 and ε represents experimental noise. For numerical calculations, we discretize Eq. (1) in a matrix form, $M = K F + \varepsilon$, where the dimensions of M, K (kernel), and F are $Nt_{de} \times 1$, $Nt_{de} \times N_{T1}$, and $N_{T1} \times 1$, respectively. Nt_{de} is represents the number of different time delays and N_{T1} is the number of different T_1. In our study, we used 200 different T_1 values from 10 ms to 1 s, which are uniformly distributed in log scale. The matrix is inverted by minimizing,

$$\text{argmin} \, \|M - KF\|^2 + \alpha \|F\|^2 \qquad (2)$$

, where $\|\cdot\|$ denotes the Frobenius norm of a matrix. The smoothness of F is controlled by α and it makes the inversion less ill-conditioned. Minimization of the first term is accelerated by a singular value decomposition (SVD) of K. Exemplary T_1 distributions in tissues of 47% and 24% prostate cancer (determined by histologic examination after T_1 measurements) are shown in Fig. 2 (a) and (b) and their fits to the experiments are shown in Fig. 2 (c) and (d).

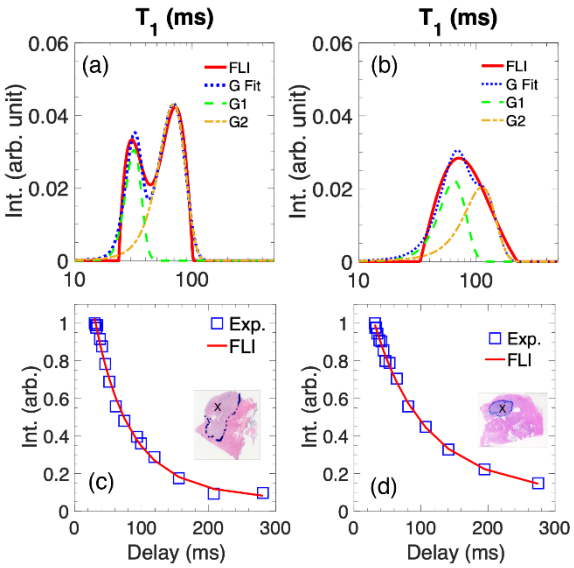

Figure 2. Exemplary fast Laplace inversion and double Gaussian fits. T_1 distributions from FLI (red solid line) in cases of 47% (a) and 24% (b) prostate cancer are shown. The Gaussian function (G1, dashed green line) with a smaller peak was chosen for T_1 distribution of cancerous prostate tissue and the other Gaussian function (G2, dash-dot golden line) represented benign prostate tissue. Their sum (G Fit, blue dotted line) was compared to the T_1 distribution from FLI. Fitting curves from FLI are compared to the experimental data in (c) and (d) where the percentages of prostate cancerous tissue are 47 and 24%, respectively. For histologic examination, the prostate tissue that underwent an NMR measurement was sectioned at every 2 mm of 4 μm thickness; and hematoxylin and eosin staining was performed. Percentage of cancerous parts (marked as 'X' in insets of (c) and (d)) in the whole tissue in each slice was used to calculate the average cancer percentage.

The T_1 distribution from FLI was then fitted to a double Gaussian function to decide T_1 of cancerous

prostate tissue. We assumed that T_1 in cancerous prostate tissue was shorter than that in benign prostate tissue.[7] Thus, the Gaussian function with smaller first moment (mean) was chosen to represent the cancerous prostate tissue. The peak was chosen as T_1 of cancerous prostate tissue and the linewidth of the selected Gaussian function was treated as an error bar for T_1 of cancerous prostate tissue. Two exemplary cases are shown in Fig. 2(a) and (b). In the case of 47% prostate cancer, Fig. 2(a), the double Gaussian successfully fits the T_1 distribution from FLI. However, the double Gaussian functions in the case of 24% prostate cancer, Fig. 2 (b), shows a limit of our method where benign prostatic hyperplasia (BPH) and prostatitis or low SNR may broaden the T1 distribution.[7]

After the T_1 measurements the samples were fixated in 10% formalin for pathological examinations and subsequently dehydrated and embedded into paraffin blocks to make 4 μm thick slices. Hematoxylin and eosin (HE) staining was used for histologic examinations (insets in Fig. 2 (c) and (d)). The percentage of cancerous tissue (PC) was averaged from each slide and the Gleason's score was determined as well. In order to examine the density of blood vessel (MVD) in the whole prostate tissue and the proliferation activity of normal and cancer cells, we performed immunohistochemical stain using formalin-fixed paraffin-embedded sections with a Benchmark XT automated staining system (Ventana Medical systems Inc.). The primary antibodies used were CD34 (1:200 DAKO, Glostrup, Denmark) and MIB-1 (1:300, DAKO). Antigens were detected using the Ventana Optiview DAB kit (Ventana Medical systems)

Results

The results of the T_1 measurements and pathological examinations in 15 pairs of the specimens are summarized in Table 1. Due to even lower SNR T_1 could not be found in specimens 1 RT, 1 LT, and 9 RT. The first number in Gleason's score represents the sum of the most common tumor grades (1 – 5) and the 2nd most common tumor grades (1 - 5). The MVD was manually calculated as the percentage of the stained area over the total area in the specimens. MIB-1 was used as a marker to determine the degree of cell proliferation and showed a range of 1 to 9%.

The comparison between T_1 and the percentage of cancerous tissue is shown in Fig. 3. T_1 from two groups, "Fresh" and "+15 Hrs", show almost identical trends which confirms negligible specimen deterioration at 4 °C for 15 hours, Fig. 3 (a). As Busch et al.'s report T_1 decreases as the percentage of cancerous part in the tissue increases.[5] Additionally, we calculated the T_1 contrast ($\delta = 1 - T_{1B} / T_{1A}$,) and difference in percentage of prostate cancer within a pair ($PC_B - PC_A$) as introduced by Busch et al. The subscript A (B) represents a sample with less (more) percentage of prostate cancer between the pair and their relationship is plotted in Fig. 3 (b). A coefficient of determination from a linear regression (R^2) was found to be 0.35 after a linear regression which was constrained to pass through the origin. The R^2 becomes 0.43 when the constraint is removed. The expected maximum δ is 0.0095 for 100% difference in percentage cancer and the increased T1 contrast compared to Busch et al.'s result (δ = 0.003 for 100%) may be attributed to the lower magnetic field of 40 μT.[7,14]

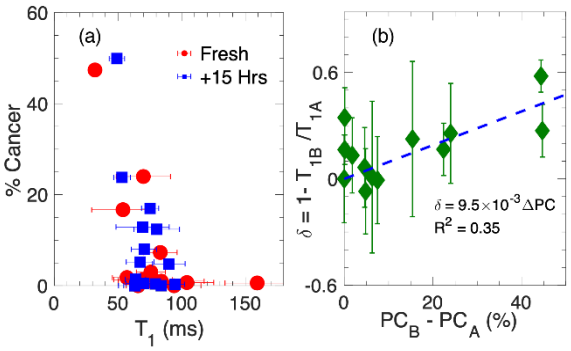

Figure 3. T_1 vs. percentage of cancerous part ($PC_{A,B}$) in tissues and T_1 contrast ($\delta = 1 - T_{1B}/T_{1A}$)

Table 1. Prostate specimens and measured results.

Specimen Num.	T_1 (ms)	δ	PC (% Cancer)	Gleason's Score	MVD (%)	MIB-1 (%)	Delay
1 RT	NA	NA	2.2	7(3+4)	8.5	1	15 Hrs
1 LT	NA		0.0	NA	11.5	1	
2 RT	76 ± 11	0.58 ± 0.09	3.0	7(3+4)	12.2	1	Fresh
2 LT	32 ± 5		47.4	7(4+3)	6.2	2	
3 RT	53 ± 7	0.17 ± 0.15	23.8	8(3+5)	22.5	6	15 Hrs
3 LT	64 ± 8		1.4	6(3+3)	19.7	1	
4 RT	84 ± 34	0.01 ± 0.43	1.0	6(3+3)	12.5	1	Fresh
4 LT	83 ± 13		7.3	7(3+4)	8.2	1	
5 RT	95 ±7	0.16 ± 0.08	0.3	6(3+3)	8.6	1	15 Hrs
5 LT	79 ± 5		0.4	6(3+3)	6.9	1	
6 RT	63 ± 9	0.00 ± 0.25	0.0	NA	13.1	1	15 Hrs
6 LT	63 ± 13		0.0	NA	9.2	1	
7 RT	104 ± 21	0.35 ± 0.17	0.7	6(3+3)	7.8	1	Fresh
7 LT	159 ± 25		0.6	6(3+3)	3.6	1	
8 RT	75 ± 7	0.06 ± 0.22	17.0	6(3+3)	9.4	1	15 Hrs
8 LT	80 ± 18		12.4	7(3+4)	7	2	
9 RT	NA	NA	0	NA	21.2	1	15 Hrs
9 LT	69 ± 21		12.9	6(3+3)	16.5	1	
10 RT	84 ± 15	-0.07 ± 0.24	0	NA	11.3	1	15 Hrs
10 LT	90 ± 13		4.8	9(4+5)	8.5	1	
11 RT	94 ± 21	0.26 ± 0.28	0	NA	26.8	1	Fresh
11 LT	70 ± 21		24	9(4+5)	17	1	
12 RT	57 ± 11	0.13 ± 0.21	1.8	6(3+3)	13.7	1	Fresh
12 LT	66 ± 9		0	NA	16.3	1	
13 RT	70 ± 14	-0.01 ± 0.25	0.5	6(3+3)	15	1	15 Hrs
13 LT	71 ± 10		8	9(4+5)	15.9	3	
14 RT	67 ± 11	0.27 ± 0.15	5.2	9(4+5)	17.8	3	15 Hrs
14 LT	49 ± 6		49.9	7(4+3)	22.8	8	
15 RT	70 ± 23	0.22 ± 0.44	1.3	6(3+3)	11.7	1	Fresh
15 LT	54 ± 25		16.7	7(3+4)	13	2	

We performed pathological measurements, Gleason's score, cell proliferation index (MIB-1 level), and MVD to understand the decrease in the T_1 in cancerous prostate tissue. The results from the measurements are shown in Fig. 4. A representative CD34 stained image is shown and one of the positively stained micro-vessels is indicated by a green arrow in Fig 4 (d).

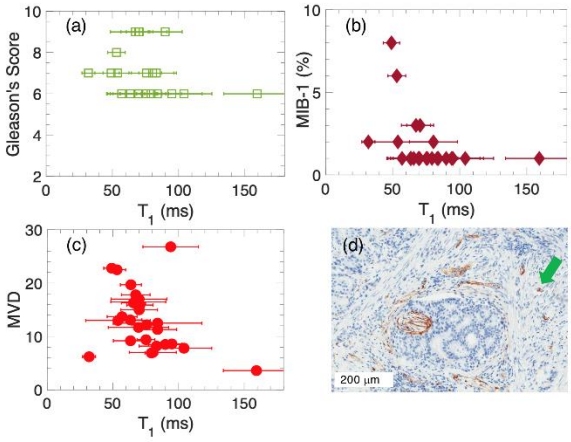

Figure 4. Comparisons between T_1 and results from the pathological examinations. Pathological examinations such as Gleason's score (a), cell proliferation marker level (MIB-1, (b)), and micro-vessel density (MVD, (c)), were compared to T_1 and shown in Fig. 4. Representative image (d) of immunohistochemical staining with CD34 antibody; brown colored areas (green arrow, one such area) indicate locations of the micro-vessels. Gleason's score was not correlated with T_1, but MVD was weakly correlated with T_1.

Gleason's score and T_1 showed no correlation, R^2 = 0.003. Structurally sensitive NMR parameters, such as T_2 or diffusion coefficients, may show more correlation with the Gleason's score.[15]

Since cell proliferation marker Ki67 and fractional T_1 change in human cervical tumor showed rather strong correlation (R^2 = 0.7), we expected similar correlation between MIB-1 and T_1.[16] However, our result of R^2 = 0.1 is inconclusive to determine the correlation between the parameters in the cancerous prostate tissue.

MVD is another potential parameter correlated with T_1. In a case of mouse ovarian cancer, in-vivo T_1 at 4.7 T increased by 16% after anti-angiogenetic treatments while MVD decreased by 59%.[17] We only measured MVD after the prostatectomies and compared a percentage of MVD with T_1 of the tissue, Fig. 4 (c). R^2 after linear regression between MVD and T_1 was 0.2, which might support a weak yet meaningful correlation. Salt resistance tests- Since the reported concentrations

Discussion

This report shows that T_1 contrast in the ultra-low magnetic fields could be enhanced in cancerous prostate tissues without contrast agents and the contrast increases with decreasing field strengths (Earth's magnetic field of 40 μT compared to 132 μT). However, unresolved T_1 distributions (Fig. 2(b)) shows the limit of our method. The might be addressed by adopting field-cycling NMR where B_p and B_o can be much higher than our B_p.[18] Once the SNR is improved, multi-dimensional NMR such as T_1-T_2 or T_1-diffusion can help correlate T_1 to cancerous prostate tissue. Additionally, finding the distribution of NMR parameters may be unnecessary if the dimension of a sample is below 1- 2 mm due to fast exchange at room temperature.[11,19]

Contrary to T_1 in cancerous prostate tissue, T_1 in other tissues (brain, liver, kidney, stomach muscle, and intestine) were reported to increase compared to that in normal tissues.[18,20,21] Increased water content, decreased macromolecular content, hypoxia, pH, and intracellular water lifetime are attributed to the increased T_1 in the cancerous tissues.[22] However, densely packed proliferating cells, irregular tumor vasculature were suggested to decrease T_1 in cancerous tissues where paramagnetic deoxyhemoglobins were accumulated.[22] Additionally, increased T_1 after anti-angiogenic treatment over a mouse ovarian cancer supports tumor vasculature plays an important role in reducing T_1 in the cancerous tissue [15]. In this section we try to explain how T_1 can be decreased in presence of paramagnetic substances such as deoxyhemoglobins in conjunction with increased MVD.

A dipolar spin interaction model may be one of the mechanisms for the suppressing of T_1 in cancerous

prostate tissue. First of all, the field dependence of dipolar relaxation rate ($1/T_{1D}$) can be expressed as in Eq. (3).

$$\frac{1}{T_{1D}} = \frac{2}{15}S(S+1)\,C_{DD}^2\left[\frac{\tau_1}{1+(\omega_S-\omega_I)^2\tau_1^2}+\frac{3\tau_1}{1+\omega_I^2\tau_1^2}+\frac{6\tau_1}{1+(\omega_S+\omega_I)^2\tau_1^2}\right], \quad (3)$$

where $C_{DD}=(\mu_0/4\pi)(\gamma_I\gamma_S\hbar)/r^3$, τ_1 is a simplified correlation time, and r is the distance between electron spin (S) and proton spin (I), and γ_S and γ_I are gyromagnetic ratio of electron and proton, respectively.[23] Unless τ_1 is extremely short (low viscosity or large diffusion coefficient), << 10-12 s, the dipolar interaction between protons and electrons explains T_1 increase ($1/T_1$ decrease) with increasing magnetic field, Eq. (3). Additionally, $1/T_{1D}$ increases as the surface density of paramagnetic ions (σs) increases.[24] This explains the necessity of large magnetic moments for higher T_1 contrast in higher magnetic fields where $1/T_{1D}$ is negligible without the moment. Gd^{3+} is one of the most popular contrast agents due to 7 unpaired electrons in the 4f orbital.[25] However, dipolar T_1 in low magnetic fields can be sensitive to even low magnetic moments. For example, in case of long τ_1 = 3.5 ns – 1 us, such as high viscosity or restricted diffusion, $T_{1D@B=3T}$ / $T_{1D@B=1mT}$ varies from 5.4 – 1500, respectively.

We conjecture that T_1 relaxation may be further accelerated by surficial relaxation due to increased micro-vessels in cancerous prostate tissue. Then, T_1 in prostate tissue may be expressed by the sum of the bulk and surface parts as T_1 in a liquid filling porous media.[24,26-29]

$$\frac{1}{T_1} = \frac{1}{T_{1,bulk}} + \varepsilon\frac{S}{V}\frac{1}{T_{1,surface}} \quad (4)$$

, where ε is the thickness of the surface layer and S/V is the surface to volume ratio.[28,29] Deoxygenated hemoglobin or other impurities near the tumor can act as paramagnetic ions such as Fe^{3+} in a case of cements.[16,22,28,30]. Increased MVD can be the source for an enhanced surface to volume ratio. Based on Eq. (3) and (4) T_1 decreases to 45 ms from bulk T_1 of 80 ms at 40 μT in a case that the surface density of paramagnetic ions is $3.0 \times 10^{11}/cm^2$, ε is 0.35 nm, τ_1 = 3.5 ns, S/V = 100 mm^{-1}. To validate above theory, it is necessary to find the surface density of paramagnetic ions or the S/V in cancerous prostate tissue.

Conclusion

We have shown that ex-vivo T_1 in cancerous prostate tissue has a larger maximum T_1 contrast at the Earth's magnetic field compared to that at 132 μT. Paramagnetic ions and the increased surface to volume ratio in vicinity of micro-vessels may be attributable to the T_1 decrease in cancerous prostate tissue. Additionally, the coil-based NMR technique we have employed is robust enough to be used in a small hospital setup but needs to be improved to achieve a higher SNR.

Acknowledgements

This work was supported by 6-1-1 grant from Korea Research Institute of Standards and Science and we appreciate Jeongseop Lee for critical reading of the manuscript.

References

1. American Cancer Society. Cancer Facts & Figures 2017. Atlanta: American Cancer Society (2017)
2. S. Verma and A. Rajesh, *AJR* Am. J. Roentgenol. **196**, S1 (2011)

3. H. U. Ahmed, A. E. Bosaily, L. C. Brown, R. Gabe, R. Kaplan, M. K. Parmar, Y. Collaco-Moraes, K. Ward, R. G. Hindley, A. Freeman, A. P. Kirkham, R. Oldroyd, C. Parker, M. and Emberton, *Lancet* **389**, 815 (2017)
4. P. Y. Poon, R. W. McCallum, M. M. Henkelman, M. J. Bronskill, S. B. Sutcliffe, M. A. Jewett, W. D. Rider, and A. W. Bruce, *Radiology* **154**,143 (1985)
5. H. Hricak, G. C. Dooms, R. B. Jeffrey, A. Avallone, D. Jacobs, W. K. Benton, P. Narayan, and E. A. Tanagho, *Radiology* **162**, 331 (1987)
6. J. O. Barentsz, J. C. Weinreb, S. Verma, H. C. Thoeny, C. M. Tempany, F. Shtern, A. R. Padhani, D. Margolis, K. J. Macura, M. A. Haider, F. Cornud, and P. L. Choyke, *Eur. Urol.* **69**, 41 (2016)
7. S. Busch, M. Hatridge, M. Mößle, W. Myers, T. Wong, M. Mück, K. Chew, K. Kuchinsky, J. Simko, and J. Clarke, *Magn. Reson. Med.* **67**, 1138 (2012)
8. A. Mohorič, and J. Stepišnik, *Prog. NMR. Spectrosc*. **54**, 166 (2009)
9. S. Manda, S. Oh, and M. D. Hürlimann, *J. Magn. Reson.* **261**, 121 (2015)
10. R. R. E. Fenrich, C. Beaulieu, and P. S. Allen, *NMR in Biomed.* **14**, 133 (2001)
11. J. R. Zimmerman, and W. E. Brittin, *J. Phys. Chem.* **61,** 1328 (1957)
12. L. Venkataramanan, Y. Q. Song, and M. Hurlimann, *IEEE Trans. on Signal Proc*.**50,** 1017 (2002)
13. Y. Q. Song, *Concepts Magn. Reson. Part A* **18,** 97 (2003)
14. J. Clarke, M. Hatridge, and M. Mößle, *Annu. Rev. Biomed. Eng.* **9**, 389 (2007)
15. C. M. Hoeks, J. O. Barentsz, T. Hambrock, D. Yakar, D. M. Somford, S. W. Heijmink, T. W. Scheenen, P. C. Vos, H. Huisman, I. M. Van Oort, J. A. Witjes, A. Heerschap, and J. J. Fütterer, *Radiology* **261,** 46 (2011)
16. P. M. J. McSheehy, C. Weidensteiner, C. Cannet, S. Ferretti, D. Laurent, S. Ruetz, M. Stumm, and P. R. Allergrini, *Clin. Cancer Res.* **16,** OF1 (2010)
17. M. K. Ravoori, M. Nishimura, S. P. Singh, C. Lu, L. Han, B. P. Hobbs, S. Pradeep, H. J. Choi, J. A. Bankson, A. K. Sood, and V. Kundra, *PLoS ONE* **10,** e0131095 (2015)
18. M. R. Ruggiero, S. Baroni, S. Pezzana, G. Ferrante, S. G. Crich, and S. Aime, *Angew. Chem. Int. Ed.* **57,** 7468 (2018)
19. S. -J. Lee, J. H. Shim, K. Kim, S.-M. Hwang, K. K. Yu, S. Lim, J. H. Han, H. Yim, J.-H. Kim, Y. S. Jung, and K. S. Kim, *Biomed. Res. Int.* **2015,** 385428 (2015)
20. R. Damadian, *Science* **171**, 1151 (1971)
21. K.-W. Huang, H.-H. Chen, H.-C. Yang, H.-E. Horng, S.-H. Liao, S. Y. Yang, J.-J. Chieh, and L.-M. Wang, *PLoS ONE* **7**, e47057 (2012)
22. T. E. Yankeelov, D. R. Pickens, and R. R. Price, *Quantitative MRI in cancer* 1st ed. (Boca Raton, CRC Press, 2011)
23. E. Belorizky, P.H. Fries, L. Helm, J. Kowalewski, D. Kruk, R. R. Sharp, and P. O. Westlund, *J. Chem. Phy.* **128**, 052315 (2008)
24. J. Korringa, D. O. Seevers, and H. C. Torrey, *Phys. Rev.* **127**, 1143 (1962)
25. L. M. De León-Rodríguez, A. F. Martins, M. C. Pinho, N. M. Rofsky, and A. D. Sherry, *J. Magn. Reson. Imaging.* **42**, 545 (2015)
26. R. L. Kleinberg, W. E. Kenyon, and P. P. Mitra, *J. Mag. Res. A* **108**, 206 (1994)
27. B. Blümich, J. Perlo, and F. Casanova, *Prog. Nucl. Magn. Reson. Spectr.* **52**, 197 (2008)
28. P. J. McDonald, J. -P. Korb, J. Mitchell, and L. Monteilhet, *Phys. Rev. E* **72,** 011409 (2005)
29. K. R. Brownstein and C. E. Tarr, *Phys. Rev. A* **19**, 2446 (1979)
30. J. P. B. O'Connor, J. H. Naish, A. Jackson, J. C. Waterton, Y. Watson, S. Cheung, D. L. Buckley, D. M. McGrath, G. A. Buonaccorsi, S. J. Mills, C. Roberts, G. C. Jayson, and G. J. M. Parker, *Magn. Reson. Med.* **61**, 75 (2009)